

Quantitative Photoacoustic Image Reconstruction for Molecular Imaging

B. T. Cox^a, S. R. Arridge^b and P. C. Beard^a

^a Department of Medical Physics and Bioengineering, University College London,
Gower Street, London WC1E 6BT, UK

^b Department of Computer Science, University College London,
Gower Street, London WC1E 6BT, UK

ABSTRACT

Biomedical photoacoustic imaging produces a map of the initial acoustic pressure distribution, or absorbed energy density, in tissue following a short laser pulse. Quantitative photoacoustic imaging (QPI) takes the reconstruction process one stage further to produce a map of the tissue optical coefficients. This has two important advantages. Firstly, it removes the distorting effect of the internal light distribution on image contrast. Secondly, by obtaining images at multiple wavelengths, it enables standard spectroscopic techniques to be used to quantify the concentrations of specific chromophores, for instance, oxy and deoxy haemoglobin for the measurement of blood oxygenation - applying such techniques directly to “conventionally” reconstructed absorbed energy maps is problematic due to the spectroscopic ‘spatial crosstalk’ effects between different tissue chromophores. As well as naturally-occurring chromophores, dye-labelled molecular markers can be used to tag specific molecules, such as cell surface receptors, enzymes or pharmaceutical agents. In QPI, a diffusion-based finite element model of light transport in scattering media, with δ -Eddington scattering coefficients, is fitted to the absorbed energy distribution to estimate the optical coefficient maps. The approach described here uses a recursive algorithm and converges quickly on the absorption coefficient distribution, when the scattering is known. By adding an area of known absorption, an unknown constant scattering coefficient may also be recovered. With optical coefficient maps estimated in this way, QPI has the potential to be a powerful tool for quantifying the concentration of molecular markers in photoacoustic molecular imaging.

Keywords: photoacoustic, molecular imaging, quantitative imaging, optical absorption coefficient

1. PHOTOACOUSTIC MOLECULAR IMAGING

In recent years, high resolution photoacoustic (PA) imaging of small animal models *in vivo* has been demonstrated.^{1,2} The presence, in tissue, of naturally occurring chromophores of interest (such as hemoglobin) as well as the increasing availability of dye-labelled molecular markers and other marker chromophores (eg. nanoshells) opens up the possibility of PA molecular imaging. The aim of PA molecular imaging is to obtain maps of the spatial distributions of the concentrations of the chromophores present in tissue. Such maps could ultimately be used to help provide insight into disease processes and aid in the development of novel drugs, in particular in conjunction with small animal models.

The absorption coefficient distribution within a medium such as tissue depends on the concentrations of the chromophores present. For j chromophores with extinction coefficient spectra $\epsilon_j(\lambda)$ and concentration distributions $C_j(\mathbf{x})$, the wavelength-dependent absorption coefficient distribution $\mu_a(\mathbf{x}, \lambda)$ may be written as a linear sum

$$\mu_a(\mathbf{x}, \lambda) = \sum_j C_j(\mathbf{x})\epsilon_j(\lambda). \quad (1)$$

Here λ is the optical wavelength, and \mathbf{x} is a position vector. If the extinction spectra of the chromophores are known, then their concentrations may be calculated from measurements of the absorption coefficient maps

Send correspondence to B. T. Cox. bencox@medphys.ucl.ac.uk

through the linear inversion of Eq. (1). This could be performed using a singular value decomposition, for instance.

Unfortunately, conventional PA imaging does not provide a map of the absorption coefficient distribution directly; it recovers an image of the initial pressure distribution following the absorption of a short laser pulse. This initial pressure distribution is proportional to the optical energy absorbed per unit volume. While this absorbed energy density distribution H does depend on the absorption coefficient distribution, the relationship is nonlinear. In general,

$$H(\lambda) \not\propto \mu_a(\lambda). \quad (2)$$

The result is that multiwavelength images of absorbed energy cannot usually be used in place of multiwavelength absorption coefficient maps in the inversion for chromophore concentrations. The nonlinearity arises because the absorbed energy density is a product of the fluence, Φ , and the absorption coefficient, and the fluence itself also depends on the absorption coefficient,

$$H(\mathbf{x}, \lambda) = \mu_a(\mathbf{x}, \lambda)\Phi(\mu_a, \mathbf{x}, \lambda). \quad (3)$$

The dependence of the fluence on the absorption distribution introduces ‘spatial crosstalk’ into the conventional PA images. For example, the spectrum of the fluence - and therefore the absorbed energy spectrum - deep inside an absorbing medium will depend on the absorption spectrum at every point through which the light has travelled.³ In a highly scattering medium, then, the spectrum of the fluence at any point will have encoded onto it the absorption coefficient spectra of much of the medium.

In order to proceed with PA molecular imaging, therefore, we first need to estimate the absorption coefficient distribution at each wavelength by removing the effect of the fluence. This problem has been called Quantitative Photoacoustic Imaging. The difficulty lies in the fact that in order to recover the absorption coefficient distribution, the fluence distribution must be known, but a calculation of the fluence distribution requires the absorption coefficient distribution that we are trying to recover. One way to tackle this problem is to improve estimates of both the absorption and the fluence distributions iteratively until both are correct. One such approach is described in Section 3 below.

2. MODELS OF LIGHT PROPAGATION

Any inversion scheme to recover an absorption coefficient map from a map of absorbed energy density will require an accurate model of light propagation in scattering media. In addition, if the inversion scheme is iterative, an efficient model would be preferable. Finally, the model must be able to calculate the fluence for any arbitrary distribution of absorption (unless the target absorber is known to be of a specific geometry, which in general will not be the case).

Monte Carlo models,⁴ which directly model the radiative transfer equation, are usually taken as the ‘gold standard’ for calculating light distributions in turbid media. For the purposes of this iterative inversion there are two drawbacks to this method. First, it is computationally intensive, and second - and more significantly - each new absorption distribution must be explicitly coded for. A model that can accept the absorption coefficient distribution as a parameter would be a much more practical choice.

One possibility is to use the finite element (FE) method to calculate numerical solutions to the diffusion approximation to the radiative transport equation. This technique is widely used in diffuse optical tomography,^{5,6} but requires that the absorption and scattering coefficients must satisfy the condition $\mu_a \ll \mu'_s$. In fact, this is true for many types of biological tissue for a useful range of absorptions. Another potential difficulty for photoacoustics is that the diffusion approximation breaks down close to where a collimated light source enters the scattering medium. Many scattering lengths from the surface the diffusion approximation is accurate, but - due to the fact that it explicitly assumes near-isotropic light sources - it does not model the highly anisotropic fluence at shallow depths. This can be ameliorated to a considerable extent through the use of the δ -Eddington approximation, which, simply by adjusting the scattering coefficients, improves the accuracy close to the surface. As this has proved a useful improvement to the FE diffusion model but is not yet widely used, its derivation is described below.

2.1. δ -Eddington Approximation

In the diffusion approximation, for a collimated light beam incident on scattering medium, the fluence at a sufficiently deep distance from the surface depends on the scattering coefficient μ_s and anisotropy parameter g only in the combination $\mu'_s = \mu_s(1 - g)$. In other words, if both μ_s and g change but the reduced scattering coefficient μ'_s stays the same, then the fluence deep within the tissue will remain the same. Close to the surface, this is not true, and changing μ_s and g , even if μ'_s remains the same, will change the fluence. This fact opens up the possibility of correcting the fluence close to the surface by increasing the anisotropy parameter g , to better model the forward-scattered light at shallow depths, while keeping μ'_s the same, so that the accuracy of the model at greater depths is not affected.

In the radiative transfer equation, the scattering of a photon from the direction $\hat{\mathbf{s}}$ to the direction $\hat{\mathbf{s}}'$ is commonly described by the angularly-independent phase function $p(\hat{\mathbf{s}} \cdot \hat{\mathbf{s}}')$, which can be written as a sum of Legendre polynomials

$$p(\hat{\mathbf{s}} \cdot \hat{\mathbf{s}}') = \sum_{l=0}^{\infty} \left(\frac{2l+1}{4\pi} \right) g_l(\mathbf{r}) P_l(\hat{\mathbf{s}} \cdot \hat{\mathbf{s}}'). \quad (4)$$

It has been found that biological tissue is well described by choosing the coefficients g_l to be $g_l = g^l$ which gives the *Henye-Greenstein* phase function, which is often seen in the equivalent but concise form $p(\hat{\mathbf{s}} \cdot \hat{\mathbf{s}}') = p(\cos \theta) = (1 - g^2)/(g^2 - 2g \cos \theta + 1)^{3/2}$. The diffusion approximation includes the first two terms of this expansion, with the coefficients $g_0 = 1$, and $g_1 = g$, the anisotropy factor.

The δ -Eddington approximation⁷ attempts to include the anisotropy of the third term of the Henye-Greenstein phase function implicitly by adjusting the scattering parameters, as described above. The Henye-Greenstein phase function is compared to the δ -Eddington phase function, in which a proportion of the light f is assumed to remain unscattered. The unscattered part can be described by including a δ -function in the phase function, $\delta(1 - \hat{\mathbf{s}} \cdot \hat{\mathbf{s}}')$, which is zero when $\hat{\mathbf{s}} \neq \hat{\mathbf{s}}'$. This δ -function may be expanded as an infinite sum of Legendre polynomials and the first three terms of this expansion are used to describe the portion f of (almost) unscattered light. The δ -Eddington phase function, then, is a combination of the first two terms in a Legendre expansion (as in the standard diffusion model but with new coefficients \hat{g}_0 and \hat{g}_1) and the first three terms of the δ -function expansion. Equating the first three terms of the Henye-Greenstein function with the δ -Eddington phase function gives

$$\sum_{l=0}^2 \left(\frac{2l+1}{4\pi} \right) g^l(\mathbf{r}) P_l(\hat{\mathbf{s}} \cdot \hat{\mathbf{s}}') = \underbrace{f \sum_{l=0}^2 \left(\frac{2l+1}{4\pi} \right) P_l(\hat{\mathbf{s}} \cdot \hat{\mathbf{s}}')}_{\approx \delta(1 - \hat{\mathbf{s}} \cdot \hat{\mathbf{s}}')} + (1-f) \sum_{l=0}^1 \left(\frac{2l+1}{4\pi} \right) \hat{g}_l(\mathbf{r}) P_l(\hat{\mathbf{s}} \cdot \hat{\mathbf{s}}') \quad (5)$$

Equating the coefficients of $P_l(\hat{\mathbf{s}} \cdot \hat{\mathbf{s}}')$ gives expressions for the new coefficients, \hat{g}_0 and \hat{g}_1 , and the factor f in terms of the old coefficient g : $\hat{g}_0 = 1$, \hat{g}_1 , renamed as the new anisotropy parameter $\hat{g} = (g - f)/(1 - f)$, and $f = g^2$. As the reduced scattering coefficient must remain unchanged we also have the requirement that $\hat{\mu}_s(1 - \hat{g}) = \mu_s(1 - g)$, which rearranges to give $\hat{\mu}_s = \mu_s(1 - f)$.

So, the δ -Eddington approximation introduces more anisotropy into the fluence close to the surface by shifting a proportion of the light into the forward direction. In practice, just two changes to the scattering coefficients are required:

$$g \rightarrow \hat{g} = (g - f)/(1 - f), \quad (6)$$

$$\mu_s \rightarrow \hat{\mu}_s = \mu_s(1 - f), \quad (7)$$

where $f = g^2$. The major advantage of this approach is that it does not require a new model to be coded, but can incorporate greater anisotropy at shallow depths, and therefore greater accuracy, with a simple change of coefficients.

An analytical solution to the diffusion approximation with δ -Eddington coefficients has been shown to agree with a MC model for a homogeneous absorbing medium.⁸ Figure 1 shows 2D maps of absorbed energy density calculated by an MC model and an FE model (incorporating the δ -Eddington coefficients) with square absorbing heterogeneities. The squares both have absorption coefficients of 1 mm^{-1} (the maximum absorption of blood at normal concentrations in the near-infrared) and the background absorption is 0.03 mm^{-1} . The scattering coefficient is set as $\mu_s = 20 \text{ mm}^{-1}$ and $g = 0.9$. The greyscales are the same in both maps and range from 0 to 14 mJ/cm^2 . The collimated tophat source, incident on the bottom of the image, has a beamwidth of 8.4 mm and a surface fluence of 1 mJ/cm . Figure 2 shows profiles through the maps in Fig. 1 and clearly shows good agreement.

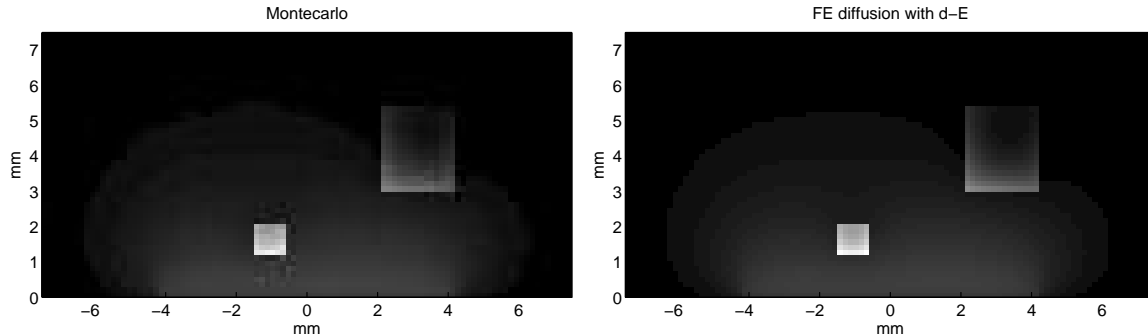


Figure 1. 2D maps of absorbed energy density calculated using Monte Carlo (MC) and diffusion with δ -Eddington finite element (FE) codes. Background $\mu_a = 0.03 \text{ mm}^{-1}$, squares $\mu_a = 1 \text{ mm}^{-1}$. $\mu_s = 20 \text{ mm}^{-1}$, $g = 0.9$. Collimated source, incident from below, with a tophat profile of width 8.4 mm and a surface fluence of 1 mJ/cm . Greyscale from 0 (black) to 14 mJ/cm^2 (white).

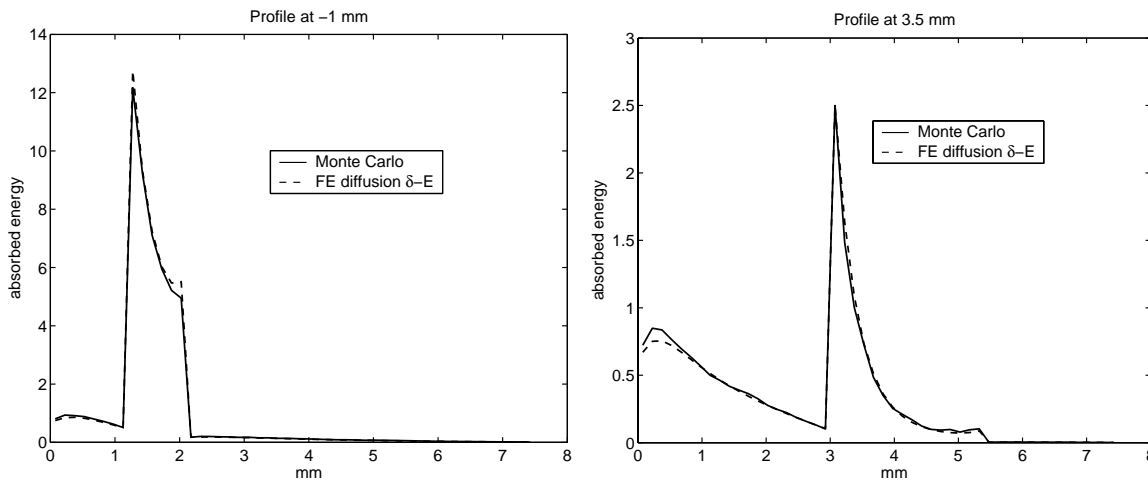


Figure 2. Profiles taken vertically through the absorbed energy images in Fig. 1 at -1 mm and 3.5 mm . Solid line: Monte Carlo, dashed line: finite element diffusion-based δ -Eddington model.

3. QUANTITATIVE PHOTOACOUSTIC IMAGING

With an accurate and computationally efficient light model, the inverse problem can now be tackled. First, a recursive method for estimating the absorption coefficient map from the absorbed energy map when the

scattering is known is described. This is followed by a scheme to invert for both the absorption coefficient map and a constant scattering coefficient by including a layer of known absorption. Both of these inversion schemes assume that the absorbed energy map can be recovered accurately and in units of absorbed energy. Neither of these assumptions presents a major limitation as conventional photoacoustic imaging algorithms that can recover the initial pressure distribution accurately (without the loss of, for instance, low frequency information) are available,⁹ and, if calibrated detectors are not available, the PA imaging system may be calibrated by imaging a phantom of known absorption.

3.1. Inversion for absorption coefficient map

If the fluence is known, then the absorption coefficient can be calculated from the absorbed energy map simply by dividing $\mu_a = H/\Phi$ (see Eq. (3)). Usually, however, the fluence is not known, and the model of light transport must be used to estimate it. To predict the fluence the scattering parameters μ_s and g are required to be known. Here it is assumed that they are. In addition, the unknown absorption coefficient map is required. As this is not yet known, it is assumed, initially, that it is zero everywhere. By including this in the model a first estimate of the fluence is obtained. Of course, the absorption coefficient map is not zero (or the absorbed energy map would also be zero) and we can find a better estimate for it by dividing the measured absorbed energy map by our first estimate of the fluence. By iterating this procedure - using the model of light transport to estimate the fluence $\Phi(\mathbf{x})$ and $\mu_a(\mathbf{x})_{k+1} = H(\mathbf{x})/\Phi(\mathbf{x})_k$ to estimate the absorption coefficient map - both $\Phi(\mathbf{x})$ and $\mu_a(\mathbf{x})$ may be recovered. When the absorbed energy map is noisy, as it will be in any actual measurements, this recursion can become unstable where the fluence is low. There are several ways to regularise the inversion to prevent this instability from dominating the solution, such as smoothing the image by filtering out the high wavenumber components, or by recovering only that part of the image where the signal-to-noise ratio is high enough. One method that regularises while preserving sharp edges in the image is to add a small regularisation parameter σ to the denominator and so use the recursion

$$\mu_a(\mathbf{x})_{k+1} = \frac{H(\mathbf{x})}{\Phi(\mathbf{x})_k + \sigma} \quad (8)$$

This inversion has been described in detail, with examples, in Cox et al.^{10,11}

3.2. Inversion for absorption coefficient map and scattering

In practice, the scattering coefficient may not be known accurately. If it can be assumed constant throughout the medium, then, by adding a layer of known absorption to the target, it is possible to invert for both the absorption coefficient map $\mu_a(\mathbf{x})$ and the constant scattering coefficient μ_s . For the example below, the layer of known absorption can be seen at the bottom of the absorption coefficient map in Fig. 4(A). The algorithm used to estimate the absorption and scattering is shown in Fig. 3. Using an initial guess for the scattering coefficient, the absorption coefficient map is estimated using the same recursion as described above (inner loop, 1). If the estimate of the absorption coefficient in the surface layer is wrong, then the scattering coefficient is changed (outer loop, 2) and the absorption calculated again. This continues until both the scattering coefficient and the absorption coefficient map have been recovered.

Many different methods could be used to update the scattering coefficient. In the example shown here, an initial guess of the scattering was chosen, and an absorption coefficient map was estimated. The scattering was then updated by an amount, $\Delta\mu_s$, proportional to the difference between the estimated absorption coefficient and the known value in the added layer, $\Delta\mu_a$,

$$\Delta\mu_s = \alpha\Delta\mu_a, \quad (9)$$

where $\alpha > 0$ determines the rate of convergence. This expression for the update works because when the scattering is too low, the fluence in the known layer will be too low (less light backscattered into it from the medium), leading to an overestimated absorption coefficient. $\alpha\Delta\mu_a$ is therefore positive and increases the scattering coefficient. Conversely, when the scattering is too high, the fluence in the known layer will be too high (too much backscattered light) and $\alpha\Delta\mu_a$ will be negative, reducing the scattering coefficient.

If the scattering coefficient is not known at all accurately, then preliminary ‘ranging’ inversions may be required in order to find an estimate close enough to the true value for the algorithm in Fig. 3 to converge. This initialisation may, for example, consist of running a number of test inversions with randomly chosen scattering coefficients, the ‘best’ value then being taken as the one for which, say, the absorption map converges most quickly, or for which the absorption coefficient and fluence stay within a certain plausible range. An alternative scheme could begin with a scattering coefficient well above its expected range which then moves down in steps until the absorption inversion converges to within sensible bounds. These preliminary inversions are simple ways of using prior knowledge of the expected ranges of the optical coefficients to find an ‘order-of magnitude’ estimate for the scattering coefficient. Once a rough estimate has been found in this way, the inversion in Fig. 3 will converge on the true value.

Figure 4 shows that the inversion in Fig. 3 works when there is no noise in the absorbed energy map. (B) shows the absorbed energy map calculated from the absorption coefficient distribution in (A). The collimated light beam, in this example, is incident upwards from the bottom with a beam width of 7 mm. (The absorbed energy map was first calculated on a 103×103 FE mesh and then linearly interpolated onto a non-coincident 50×50 mesh for the reconstruction, to mitigate the ‘inverse crime’ of simulating and inverting data on the same

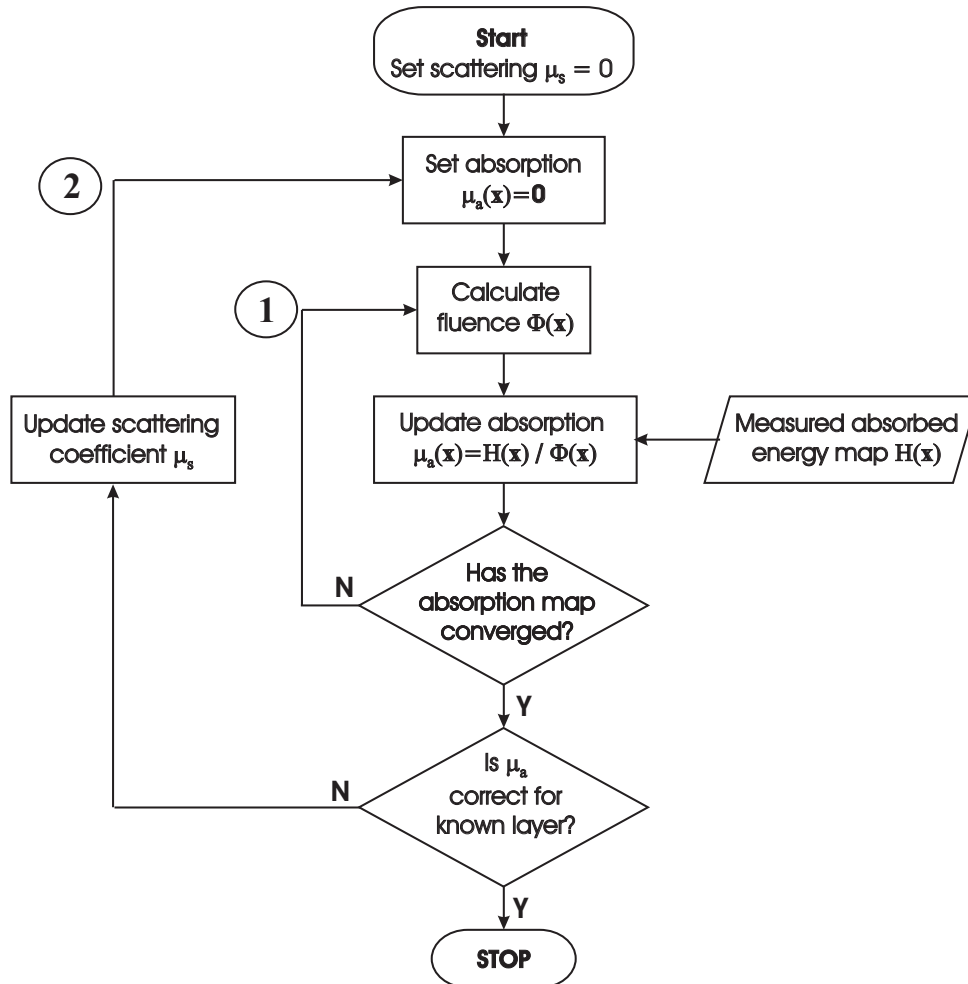


Figure 3. Flowchart showing the quantitative photoacoustic imaging algorithm to recover an absorption coefficient map and a constant scattering coefficient from an absorbed energy map, the image generated using conventional photoacoustic imaging.

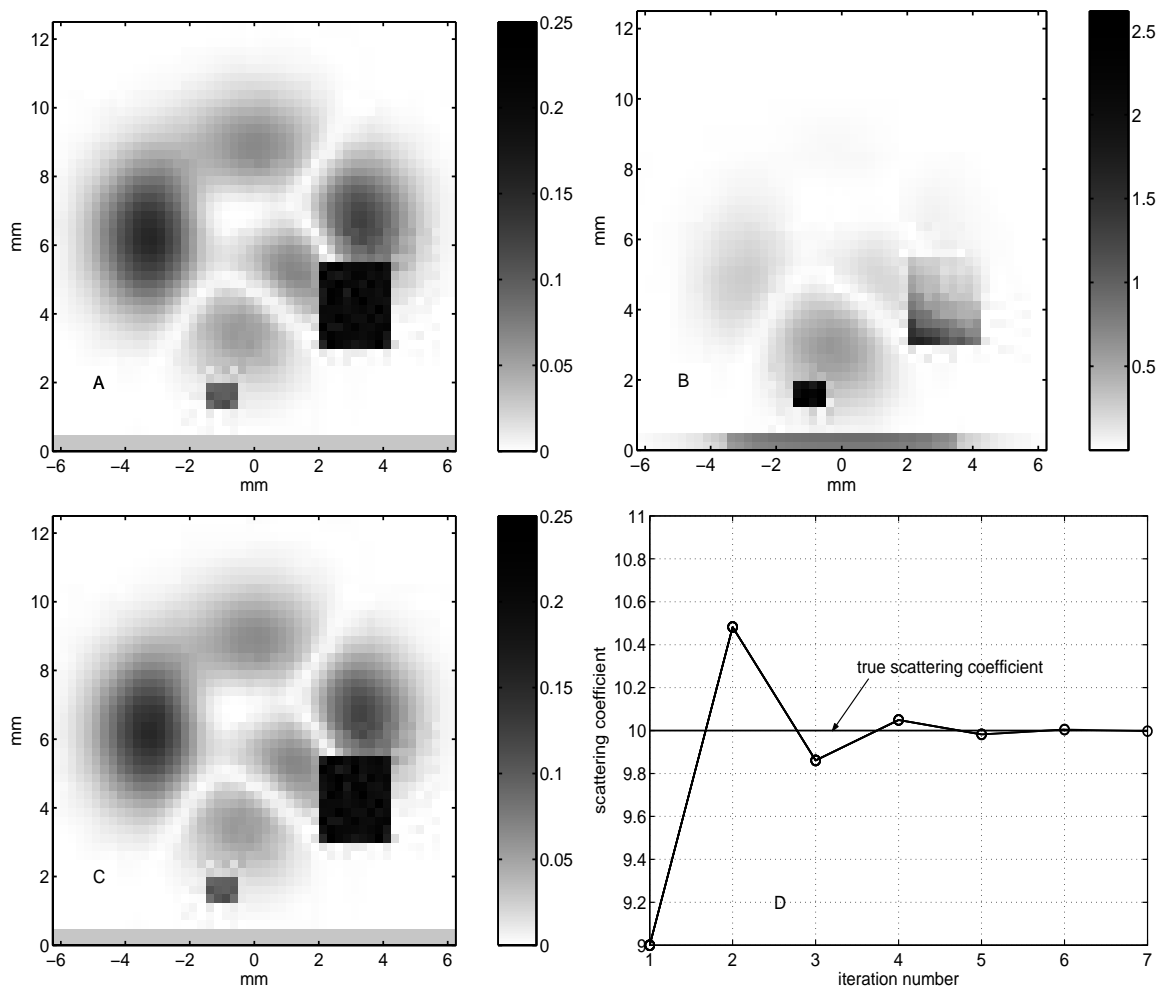


Figure 4. Quantitative reconstruction of an absorption distribution $\mu_a(\mathbf{x})$ and a constant scattering coefficient, μ_s , using data simulated using a FE model of light transport. Noise-free case. (A) true absorption coefficient distribution, greyscale from 0 to 0.25 mm⁻¹, with a layer of known absorber (0.05 mm⁻¹) along the bottom edge where the light enters the medium, (B) map of absorbed energy density (ie. the conventional PA image), greyscale from 0 to 2.6 mJ/cm², collimated source incident from below, beamwidth 7mm and surface fluence 1 mJ/cm, (C) recovered absorption coefficient distribution, greyscale from 0 to 0.25 mm⁻¹, (D) estimated scattering coefficient (cm⁻¹) as a function of iteration number, true $\mu_s = 10$ cm⁻¹.

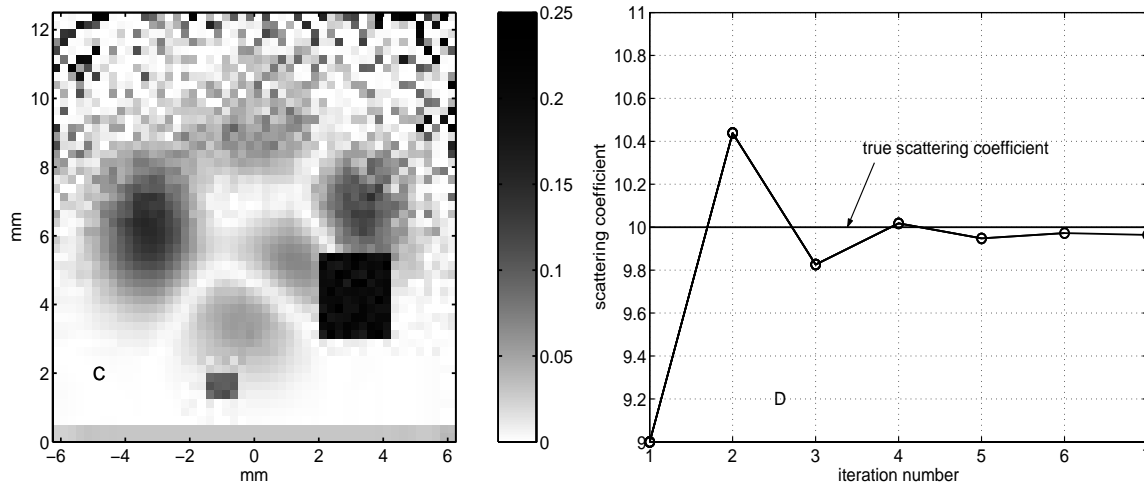


Figure 5. Quantitative reconstruction of an absorption distribution $\mu_a(\mathbf{x})$, and a constant scattering coefficient, μ_s , using data simulated using a FE model of light transport as in Fig. 4, but containing noise (SNR 40 dB close to, and down to -20 dB furthest from, the source). Regularisation parameter $\alpha = 1e - 4$. (C) recovered absorption distribution, greyscale from 0 to 0.25 mm⁻¹, (D) estimated scattering coefficient (cm⁻¹) as a function of iteration number, true $\mu_s = 10 \text{ cm}^{-1}$.

grid.) The constant scattering coefficient (D) and the absorption coefficient map (C) have both been recovered accurately. To generate Figure 5, the same absorbed energy map was used as in Fig. 4, but random noise was added to the image resulting in a signal-to-noise ratio, defined as $10 \log(\text{absorbed energy}/\text{noise})$, ranging from about 40 dB where the light enters the tissue to -20dB on the far side of the simulated phantom. Even in this noisy case, the inversion has recovered the absorption coefficient map (to a depth of about 8 mm) and the constant scattering coefficient to within a few per cent of their true values.

4. CONCLUSIONS

Photoacoustic molecular imaging has the potential to provide quantitative, high resolution, 3D images of the spatial distribution of concentrations of both endogenous and exogeneous chromophores, including those tagged to highlight a particular bio-molecule (such as an enzyme or mRNA), especially in small animal models. However, before this is possible it is necessary to solve the large inverse problem of quantitative photoacoustic imaging: estimating the absorption and scattering coefficient distributions from conventional photoacoustic images of absorbed energy density. That is to say, in order to “pick out” a specific chromophore from a spectrally corrupting background absorption (eg, to be able to detect and quantify a targeted contrast agent within a background of hemoglobin) it is first necessary to obtain absorption coefficient maps as a function of optical wavelength. Here we have presented an incremental step on the way to achieving such inversions by inverting for an absorption map and a constant scattering coefficient from a one-wavelength image. The technique has been shown to work on noisy simulated data.

ACKNOWLEDGMENTS

This work was supported by the Engineering and Physical Sciences Research Council, UK.

REFERENCES

1. X. Wang, Y. Pang, G. Ku, X. Xie, G. Stoica, and L. V. Wang, “Noninvasive laser-induced photoacoustic tomography for structural and functional in vivo imaging of the brain,” *Nature Biotech.* **21**(7), pp. 803–806, 2003.

2. R. Kruger, W. Kiser, D. Reinecke, G. Kruger, and K. Miller, "Thermoacoustic optical molecular imaging of small animals," *Molecular Imaging* **2**, pp. 113–123, 2003.
3. J. Laufer, C. Elwell, D. Delpy, and P. Beard, "Spatially resolved blood oxygenation measurements using time-resolved photoacoustic spectroscopy," *Oxygen Transport to Tissue XXVII, Series: Advances in Experimental Medicine and Biology* **578**, pp. 155–160, 2006.
4. S. L. Jacques and L. Wang, *Monte Carlo Modeling of Light Transport in Tissues in Optical-Thermal Response of Laser-Irradiated Tissue*, Eds. A. J. Welch and M.J.C. van Gemert, Plenum Press, New York, 1995.
5. S. Arridge, M. Schweiger, M. Hiraoka, and D. Delpy, "A finite element approach for modelling photon transport in tissue," *Medical Physics* **20**, pp. 299–309, 1993.
6. M. Schweiger, S. Arridge, M. Hiraoka, and D. Delpy, "The finite element method for the propagation of light in scattering media: Boundary and source conditions," *Medical Physics* **22**, pp. 1779–1792, 1995.
7. T. Spott and L. O. Svaasand, "Collimated light sources in the diffusion approximation," *Appl. Opt.* **39**(34), pp. 6453–6465, 2000.
8. J. G. Laufer, C. Elwell, D. Delpy, and P. Beard, "In vitro measurements of absolute blood oxygen saturation using pulsed near-infrared photoacoustic spectroscopy: accuracy and resolution," *Phys. Med. Biol.* **50**, pp. 4409–4428, 2005.
9. K. P. Köstli, M. Frenz, H. Bebie, and H. P. Weber, "Temporal backward projection of optoacoustic pressure transients using Fourier transform methods," *Phys. Med. and Biol.* **46**(7), pp. 1863–1872, 2001.
10. B. T. Cox, S. Arridge, K. Köstli, and P. Beard, "Quantitative photoacoustic imaging: fitting a model of light transport to the initial pressure distribution," *Proc. SPIE* **5697**, pp. 49–55, San Jose, 2005.
11. B. T. Cox, S. R. Arridge, and P. C. Beard, "2D quantitative photoacoustic image reconstruction of absorption distributions in scattering media using a simple iterative method," *Appl. Opt.* **45**(8), pp. 1866–1874, 2006.